Analysis of the electrically stimulated acoustic-wave method for observing space charge in semi-insulating films

Joseph B. Bernstein
Massachusetts Institute of Technology, Lincoln Laboratory, 244 Wood St., Lexington, Massachusetts 02173
(Received 8 April 1991)

The electrically stimulated acoustic-wave (ESAW) method for observing resident space charge in dielectric insulators has been used to characterize the poling behavior of millimeter-thick samples of polymeric insulation. The principle involves applying a voltage pulse across a material containing space charge and recording the exiting stress-wave signal by means of a piezoelectric transducer. This is a noninvasive technique and may be performed, *in situ*, during any space-charge-generating experiment. This method is able to detect space charge with a figure of merit equal to the sensitivity times the resolution of 130 pC/cm^2, and, to our knowledge, is the lowest reported for any nondestructive space-charge-profiling technique.

I. INTRODUCTION

The accumulation of bulk space charge due to an externally applied field is of concern for the characterization of nearly any semi-insulating material. Space-charge-limited currents give many details concerning the density of states and the contact dynamics.[1–5] However, one cannot observe the space-charge distribution across a sample using purely electrical means. Consequently, there have been many efforts to obtain space-charge information in dielectric films.[6,7]

The electrically stimulated acoustic-wave (ESAW) method for profiling the space charge distribution in an acoustically homogeneous material has been developed and shown to work with millimeter-thick samples of polymeric insulation.[8–13] The technique is noninvasive, allowing it to be performed simultaneously with any space-charge-generating experiment. Two methods of generating space charge, in order to observe the effects with ESAW, have been used. One method was a dc voltage application over several days[9] and a second was a shallow electron-beam implantation near one boundary.[10] In both experiments, the ESAW method gave time resolved space charge distribution profiles.

This method was presented by Takada, Maeno, and Kushibe[12] in 1985 as the electroacoustic-pulse method. The process of determining the charge profile from a recorded acoustic signal received by the transducer uses a simple signal processing algorithm as described in a publication by Maeno *et al.*[13]

A representation of the basic apparatus is illustrated in Fig. 1. This schematic shows the setup used for profiling thick poly(methylmethacrylate) samples in previous studies. The delay line acts as a common ground. dc voltage is applied to the top electrode and the transducer output is detected from within the brass housing. The transducer is electrically enclosed to reduce the noise resulting from external sources. The signal output from the transducer is fed out through a BNC connector. The signal is then detected by a digital recording scope that is triggered by the voltage pulse generator.

The principles described in this paper are completely general and may be applied to thin films and materials with high acoustic velocities as long as the detection equipment is fast enough to resolve the incoming signals. The next section describes the method and how it is able to measure charge layer distributions in a material of arbitrary thickness. Then, a review of one-dimensional acoustic propagation will be presented as it applies to designing an ESAW apparatus. A basic treatment of the electrical response of an acoustic transducer to an impinging stress signal follows in a subsequent section and the stress-wave generation in the insulating film due to a voltage pulse is treated in the section after that. Finally, some calibration results which demonstrate the effectiveness of the technique will be presented as well as

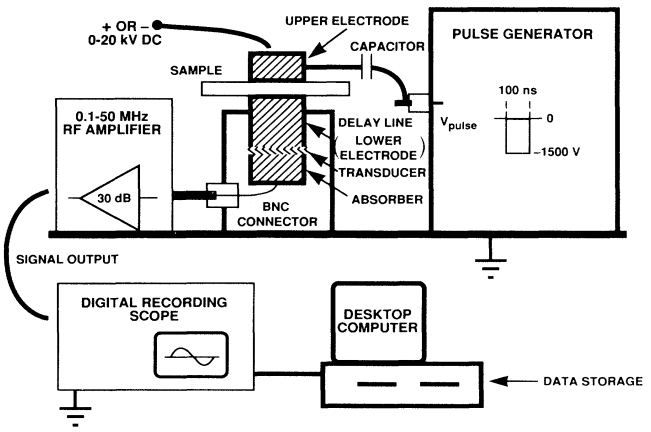

FIG. 1. Schematic of the low-frequency experimental ESAW setup.

some comments regarding the application to deposited thin films.

II. ESAW METHOD

The ESAW detection scheme is based on the Lorentz force law in one dimension. An externally applied pulse field induces a perturbation force density on the material in the presence of resident charge. The perturbation launches an acoustic wave which originates from the charged bulk. Propagation will be assumed to occur along the z axis, while the x-y plane will be considered infinite in extent. All spatial variations, therefore, are in the z dimension.

A time-dependent mechanical force density (F_0) results from the charge density $\rho_q(z)$ at every point within the sample times the perturbing Laplacian field $E_z(t)$,

$$F_0(z,t) = \rho_q(z)E_z(t), \tag{1}$$

which is the driving force that propagates a stress wave $T_z(z,t)$ from every point across the sample ($0 < z < d$). The acoustic path is indicated in Fig. 2, showing the relative positions of the sample, acoustic delay line, and the piezoelectric transducer.

If a perturbation field is much shorter than the relaxation time of the material, then trapped charges can be considered fixed in the time frame of the pulse. If the voltage pulse is also sufficiently short by comparison to the propagation of the resulting stress wave, the excitation can be said to occur in a $\delta(t)$, using the Dirac δ function at time, $t = 0$, so

$$E_z(t) \approx \frac{V_p}{d}\Delta t\delta(t), \tag{2}$$

where Δt is the effective pulse width and $\Delta t\delta(t)$ is the dimensionless short-duration-time representation of the pulse envelope. The relation (1) describes the time-dependent fraction of the nonequilibrium force, launching an acoustic wave that can be detected by a piezoelectric transducer on the other side of the lower electrode.

The stress signal produced by a charge density excited by the suddenly applied perturbation field, $E_z(t)$, propagates away from the source at the velocity of sound v_s.

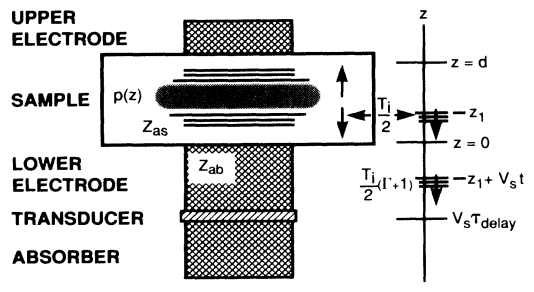

FIG. 2. Simplified acoustic model of a charge layer of density $\rho_q(z)$ under the influence of an E field $E_z(t)$, causing a stress $T_i(z,t)$ to propagate outward through the electrodes.

Immediately after the field is removed, the charge density returns to its equilibrium position. The resulting acoustic time signal is related to position by the velocity of sound within the sample,

$$z_{\rm rel}(t) = v_s t, \tag{3}$$

where $z_{\rm rel}(t)$ is the relative position in the sample with respect to the lower electrode boundary, since the signals are detected from the lower to the upper electrode. The delay time for a signal to propagate from the lower electrode boundary to the detector is $\tau_{\rm delay}$. This is the relative position due to the adjusted time, $t = t' - \tau_{\rm delay}$, where t' represents the time after the pulse is applied. Thus, $z_{\rm rel}$ across the sample corresponds to the time between the electrodes $0 \leq z_{\rm rel} \leq d$.

The detector response to a surface sheet charge is taken as the impulse response $e(t)$ at time, $t = 0$, after the acoustic coupling delay, $\tau_{\rm delay}$, as seen in Fig. 2. The detector then responds to each arriving differential element of signal resulting from the charge distribution, generating a voltage signal $V_i(t)$ which is detected by the recording scope

$$V_i(t) = K\int_0^t \frac{V_p}{d}\rho_q\left(\frac{z}{v_s} - \tau_{\rm delay}\right)p(t)v_s dt, \tag{4}$$

where the time-dependent pulse envelope $p(t)$ is defined by the shape of the electrical excitation

$$e(t) = \frac{V_p}{d}p(t) \tag{5}$$

and the trace output corresponds in time to the charge distribution in space.

If the detector response is not perfectly flat within the frequency domain of the signal, some signal processing will be required to correlate the received electrical signal with the acoustic wave to find the charge profile. A double Fourier transform is performed on the output signal, maintaining both real and imaginary components. Using the principle

$$f(t - t_0) \Longleftrightarrow F(\omega)e^{j\omega t_0} \tag{6}$$

to transform the output signal, one can recover the charge distribution after division by the transform of the unshifted impulse response. The transform of (4) is

$$V_i(\omega) = \frac{KV_p v_s}{j\omega d}(1 - e^{-j\omega\Delta t})e^{j\omega\tau_{\rm delay}}R_q\left(\frac{\omega}{v_s}\right), \tag{7}$$

where $R_q(k_z)$ is the spatial transform of the charge distribution. The linear acoustic dispersion relation,

$$\omega = v_s k_z, \tag{8}$$

allows a one-to-one mapping of the time domain signal into a spatial distribution.

The same analysis can be performed in the frequency domain by applying a steady-state voltage $V_p(\omega)$ as the test signal and sweep in frequencies. The resulting output can then be substituted for the Fourier transform of the detected signal, R_q in (7).

III. PROPAGATION

This section reviews some principles of one-dimensional acoustic propagation as related to signal detection. In order to maintain a consistent set of electrical and elastic terms, the conventions used in the text by Kino[15] have been adopted. The stress, strain, and velocity of sound are represented by T, S, and v_s, respectively, while u, $\dot{u}$, and $\ddot{u}$ are particle displacement, velocity, and acceleration. The force density in the material bulk is

$$\rho_{m0}\ddot{u} = \frac{\partial T_z}{\partial z} + F_0(z,t), \tag{9}$$

where ρ_{m0} is the specific mass density. The linear stress in a material is defined in one dimension as

$$T_z = \mathcal{E}\frac{\partial u}{\partial z}, \tag{10}$$

where $\mathcal{E}$ is the Young's modulus of the material, which can be substituted back into (9) to yield the wave equation with a temporal and spatial excitation

$$\frac{\partial^2 u}{\partial t^2} = v_s^2\frac{\partial^2 u}{\partial z^2} + \frac{F_0(z,t)}{\rho_{m0}} \tag{11}$$

and the velocity of sound

$$v_s = \sqrt{\mathcal{E}/\rho_{m0}}, \tag{12}$$

which is the velocity at which stress and strain waves travel through the material.

Solutions of (11) are found for all time and space after the stress at every point z has been determined at time $t = 0$. In this one-dimensional system, a signal may only propagate in two directions; T_z^+ for the $+z$-directed, and T_z^- for the $-z$-directed stress signals. Since the transducer is located in the $-z$ direction, only the signal propagating in that direction is considered,

$$T_z(z,t) = T_z^-\left(z', t - \frac{z'-z}{v_s}\right), \tag{13}$$

where z' indicates the position of the charge density, in reference to an observer at z.

The initially generated stress will be defined here as

$$T_i(z)_{t=0} = v_s\frac{V_p\Delta t}{d}\rho_q(z) \tag{14}$$

for the propagation of a signal from its initial position within the sample, as illustrated in Fig. 2. The signal which propagates towards the lower electrode is

$$T_z(z,t) = \frac{T_i(z+v_s t)}{2} \tag{15}$$

impinging at the sample-electrode interface and transmitted toward the detector.

The reflection coefficient for a signal propagating from material 1 toward material 2, Γ_{12}, is determined by the ratio of reflected stress T_{r1} to incident stress T_{i1} at the interface

$$\Gamma_{12} = \frac{T_{r1}}{T_{i1}} = \frac{Z_{a2}-Z_{a1}}{Z_{a2}+Z_{a1}}, \tag{16}$$

where the specific acoustic impedance Z_a is defined[15] as

$$Z_a = \rho_{m0}v_s = \sqrt{\rho_{m0}\mathcal{E}} \tag{17}$$

which is a material property.

The transmission coefficient of the interface, T_{12}, is found from conservation of stress in elastic media

$$T_{12} = \frac{2Z_{a2}}{Z_{a1}+Z_{a2}} = 1 + \Gamma_{12} \tag{18}$$

which is positive for all values of Z_{a1} and Z_{a2}. What is interesting from this relation is that zero transmission results from a negative unity reflection coefficient and the transmitted stress is double the incident stress with positive unity reflection.

A detector that is perfectly matched to the delay line will generate no reflections at that interface; thus, all of the signal in the delay line contributes to the voltage output. Using a method described by Haus and Melcher[16] to visualize signal propagation, a two-dimensional z-t plot of the stress wave is illustrated in Fig. 3. In this figure, one can see how a time domain signal contains spatial information originating between the electrodes.

By following the line of constant z at the detector, one can visualize the arrival of an excitation originating from the lower surface, $z = 0$, after τ_{delay} and from the upper surface, $z = d$, after an additional time d/v_s. The incident stress is reflected at the interface with a coefficient Γ and transmitted with $(1 + \Gamma)$. The transmitted signal, in this example, propagates with a higher velocity of sound in the delay line than in the sample, so the slope in the lower portion of Fig. 3 is broader. The characteristics of the signal originating within the sample are preserved as they propagate through the delay line, as long as diffraction and acoustic attenuation remain negligible.

IV. TRANSDUCER

The piezoelectric acoustic transducer used in the ESAW system converts stress waves into electrical signals by producing a voltage across the stress-sensitive media. Signals produced by the transducer are amplified

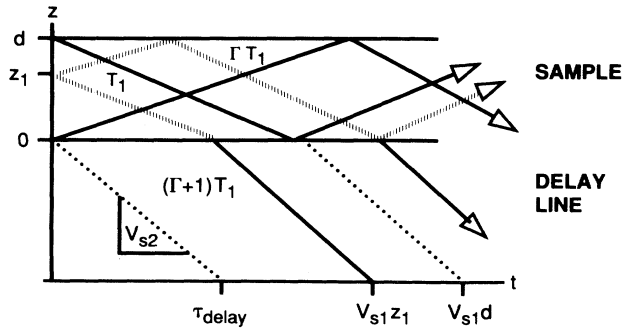

FIG. 3. Plot of position vs time for an impulsive stress T_i originating at z_1, propagating at v_{s1} in the sample, and v_{s2} in the brass delay line.

and sent to a recording oscilloscope that stores the signal wave form with respect to time. Acoustic information enters the crystal from the *front* and either exits the *back* into an absorbing material or is reflected back into the transducer. For the remainder of this discussion, front and back will refer to the crystal surfaces while top and bottom refer to the sample. Also, the term *crystal* will be used interchangeably with transducer.

For the purpose of understanding how to design an optimal transducer for ESAW measurements, a simplified analysis of longitudinal mode, linear, time-invariant acoustic detection will be presented. A systems approach will provide a method for visualizing the detection of first arrival pulses by knowing the frequency response of the crystal through Fourier decomposition of the response to an impulsive stress.

A. Constitutive relations

In order to represent the electrical response of the transducer to an acoustic wave, the behavior may be considered in one dimension using the first-order, linear, constitutive relations for a piezoelectric. Consider the relation for dielectric displacement $\mathbf{D}$ with a permittivity ϵ, and local piezoelectric polarization $\mathbf{P}_p$,

$$\mathbf{D} = \epsilon \mathbf{E} + \mathbf{P}_p. \tag{19}$$

In a piezoelectric material, the internal polarization is proportional to the stress

$$P_p(z) = \epsilon g_{33} T_z(z), \tag{20}$$

where g_{33} is the z-directed field constant for z-directed stress.[15] If the crystal is assumed homogeneous and charge neutral, Gauss's law states

$$\nabla \cdot \mathbf{D} = 0 \tag{21}$$

resulting in

$$E_z(z) = -\frac{1}{\epsilon} P_p(z) = -g_{33} T_z(z) + \text{const}, \tag{22}$$

where the constant must satisfy the surface boundary conditions.

The local z-directed electric field $E_z(z)$ is proportional to the stress at position z in the bulk of the piezoelectric material. The open-circuit voltage across the transducer at a given time is

$$V_i(t) = -\int E(z,t)dz = g_{33} \int_{z=0}^{L_t} T_z(z,t)dz \tag{23}$$

for the transducer thickness

$$L_t = v_{st} \tau_a \tag{24}$$

with v_{st} and τ_a as the velocity of sound and transit time across the transducer.

Under short-circuit conditions, $V_i(t) = 0$. The transducer current i_t is found by

$$i_t(t) = C_0 \frac{dV_i}{dt} = C_0 g_{33} \int_{z=0}^{L_t} \frac{d}{dt} T_z(z,t)dz, \tag{25}$$

where C_0 is the effective capacitance of the transducer. One can therefore model the crystal as a voltage source with an inherent capacitance due to its geometry and permittivity ϵ where

$$C_0 = \frac{\epsilon A_t}{L_t} \tag{26}$$

for a transducer area A_t.

The transducer capacitance is connected to the detector, having electrical impedance Z_{e0}, assumed here to be dominated by the resistive input impedance of the amplifier

$$Z_{e0} \approx R_0. \tag{27}$$

A first-order Thevenin equivalent model of the electrical output network for the piezoelectric voltage source in series with a single capacitor and resistor is shown in Fig. 4. This first-order high pass filter with electrical time constant, $\tau_e = R_0 C_0$, and output voltage V_0 across the resistor represents the transducer response to a stress signal input.

The voltage signal detected by the amplifier and recorded by the scope is found by solving for $V_0(t)$,

$$V_0(t) = \tau_e \frac{d}{dt} [V_i(t) - V_0(t)], \tag{28}$$

an expression that is easily transformed into frequency domain. Once the solution is found for all conditions of τ_e and $V_i(\omega)$, the time domain impulse response is recovered by taking the inverse Fourier transform.

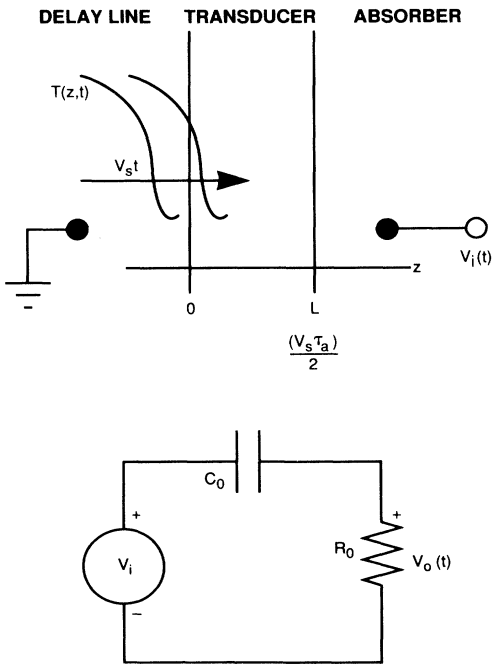

FIG. 4. Schematic of the piezoelectric transducer and the resulting voltage signal $V_i(t)$ which drives the RC circuit to produce the detected signal $V_0(t)$.

B. Signal response

Acoustic signal reception is affected by two time constants and by possible reflections from the boundaries of the crystal. The acoustic time constant τ_a is the single trip time for an acoustic signal to move across the transducer. The electrical time constant τ_e is the RC product of the crystal in series with the amplifier. As for the transducer mounting, three configurations are possible: a system where the transducer is acoustically matched on both faces, a system where the front is matched and the back is open, and one where neither side is matched. The third case results when the delay line and transducer materials are selected without regard to matching the acoustic impedances.

Plane-wave propagation, without diffraction, dispersion, or loss, will be assumed for simplicity of understanding propagation in this system. Furthermore, the bonds between the metal and piezoelectric crystal will be considered negligibly thin, so a material interface would be characterized by a single reflection coefficient Γ. Two interfaces are present at the detector, one at the transducer front and one at the back, two reflection coefficients therefore characterize the boundary effects. The front reflection coefficient will be referred to as Γ_a and is the amount returning into the delay line as the stress wave enters the crystal while Γ_b is the amount reflected back into the crystal at the back interface.

A quasistatic approach to understanding transducer operation is appropriate for broad-band crystals (low Q), operated far from resonance, receiving purely planar waves. At or near the resonant frequency of a bulk wave transducer, the response may be influenced by second-order effects which will not be discussed here.

The Fourier transform of the high-pass filter described by (28) results in the transfer function

$$\frac{V_0(\omega)}{V_i(\omega)} = \frac{j\omega\tau_e}{1+j\omega\tau_e}, \tag{29}$$

where $\tau_e = RC$. This relation is independent of the acoustic transit time τ_a. The thickness of the transducer is inversely proportional to the capacitance. The two time constants depend on the material, area, and amplifier input impedance, but will be treated independently for now.

The transducer produces a frequency-dependent open-circuit voltage by integrating stress across its thickness (23) which is then detected through the RC filter (28). The time-domain output is the convolution of these two functions, which is the inverse Fourier transform of the product in frequency space. The received voltage signal V_0 depends on the frequency characteristics of the acoustic signal and the mechanical termination at both ends. The following are the three general cases of transducer output functions based on their acoustic termination.

1. *Matched transducer*

A perfectly matched system is one with equal acoustic impedances on either side of the transducer so it does not reflect any signal at either boundary:

$$\Gamma_a = \Gamma_b = 0. \tag{30}$$

The frequency domain representation of the output voltage for an arriving stress signal is found through the Fourier transform of (23),

$$\frac{V_i(\omega)}{T(\omega)} = 2\frac{g_{33}v_s}{j\omega}\sin\left(\frac{\omega\tau_a}{2}\right)e^{-j\omega\tau_a/2}, \tag{31}$$

where the exponential term results from the time delay across the transducer. This transfer function is only intuitively helpful under certain limiting cases. In the low-frequency limit, $\omega\tau_a \ll 1$, the sine function may be approximated by its argument. Hence, the magnitude of (31) reduces to

$$\left|\frac{V_i}{T}\right|_{\omega\tau_a\to 0} = g_{33}v_s\tau_a. \tag{32}$$

When the acoustic transfer function is combined with the electrical response, the output for a steady-state signal whose frequency is much lower than τ_a,

$$A(\omega) = \left|\frac{V_0(\omega)}{T(\omega)}\right| = g_{33}v_s\tau_a\frac{\omega\tau_e}{\sqrt{1+(\omega\tau_e)^2}}, \tag{33}$$

and is independent of τ_a. This states that the voltage output is independent of frequency as long as $\tau_e^{-1} \ll \omega \ll \tau_a^{-1}$.

The system response at frequencies greater than the inverse acoustic time constant is found from the time domain response function (23) once again. An acoustic wave form propagating through the transducer at an instant of time may be decomposed into a superposition of normal acoustic modes,

$$T(t) = \sum_{n=0}^{\infty} C_n \sin\left(\frac{n\pi}{\tau_a}t\right), \tag{34}$$

for the components C_n that solve $T(t)$ at a fixed point in space. We are only interested in the region between 0 and τ_a since that is the portion of the signal integrated in (23) giving a voltage output. Consequently, the frequency domain representation is a series of impulses

$$T(\omega) = \sum_{n=1}^{\infty} C_n \delta\left(\omega - \frac{n\pi}{\tau_a}\right) \tag{35}$$

at integer multiples of the fundamental frequency.

The frequency domain response of the open circuit crystal voltage V_i may be found at each frequency, $k_n = n\pi/\tau_a$, for a stress signal $T(\omega)$, from (31) which results in the expression

$$V_i(\omega) = \sum_{n=1}^{\infty} \frac{g_{33}v_sC_n}{jk_n} 2\sin\left(\frac{n\pi}{2}\right)e^{-jn\pi/2} \tag{36}$$

having values of $(0, \pm 1)$ for the sine function. Therefore, the magnitude of the open circuit voltage is inversely proportional to the frequency. The output function for a specific input stress wave in frequency space for $\omega \gg \tau_a^{-1}$

is approximately

$$A(\omega) = \left|\frac{V_0(\omega)}{T(\omega)}\right| = \frac{g_{33}v_s\tau_e}{\sqrt{1+(\omega\tau_e)^2}}, \tag{37}$$

where a flat response is seen for $\tau_e^{-1} \gg \omega \gg \tau_a^{-1}$.

The relations (33) and (37) together give the complete asymptotic frequency domain picture for both limiting cases, shown in Figs. 5(a) and 5(b) for all frequencies. This representation illustrates the scaled response to different frequency components making up a time-resolved signal.

2. *Open-back transducer*

The second configuration is a transducer that is matched on the front side but open on the back ($Z_2 = 0$), so any signal which impinges on the back surface is reflected with equal magnitude but opposite sign, Γ_a=0 and Γ_b=−1. The signal reflected to the front returns, unimpeded, to the lower electrode. In the time domain, this configuration subtracts the integral of the delayed returning signal from the integral of the arriving signal.

$$V_i(t) = g_{33}v_s\left(\int_{t=0}^{\tau_a} T_z(z,t)dt - \int_{t=\tau_a}^{2\tau_a} T_z(z,t)dt\right). \tag{38}$$

When transformed into frequency space, the result is similar to (31) with the sine term squared:

$$\frac{V_i(\omega)}{T(\omega)} = \frac{g_{33}v_s}{j\omega}4\sin^2\left(\frac{\omega\tau_a}{2}\right)e^{-j\omega\tau_a}. \tag{39}$$

By direct analogy to the matched transducer relation (31), the output response for low frequencies $\omega\tau_a \ll 1$ will be

$$A(\omega) = g_{33}v_s\tau_a^2\frac{\omega^2\tau_e}{\sqrt{1+(\omega\tau_e)^2}} \tag{40}$$

and is proportional to ω^2 for $\omega\tau_e \ll 1$. The inverse transform of (40) is proportional to the second derivative. An open-backed setup has a fast gain fall-off for low frequencies. Consequently, it will yield poor resolution of low-frequency components.

The response to high frequencies is found following the same method described previously. Since the sine term is squared, the components C_n are multiplied by either 1 or 0 when substituted back in (39). Figures 5(c) and 5(d) illustrate the response of an open-backed transducer for the two limiting cases. The high-frequency responses are the same as for the matched transducer. A narrow pulse whose width is much shorter than crystal acoustic thickness τ_a is not influenced by the back side termina-

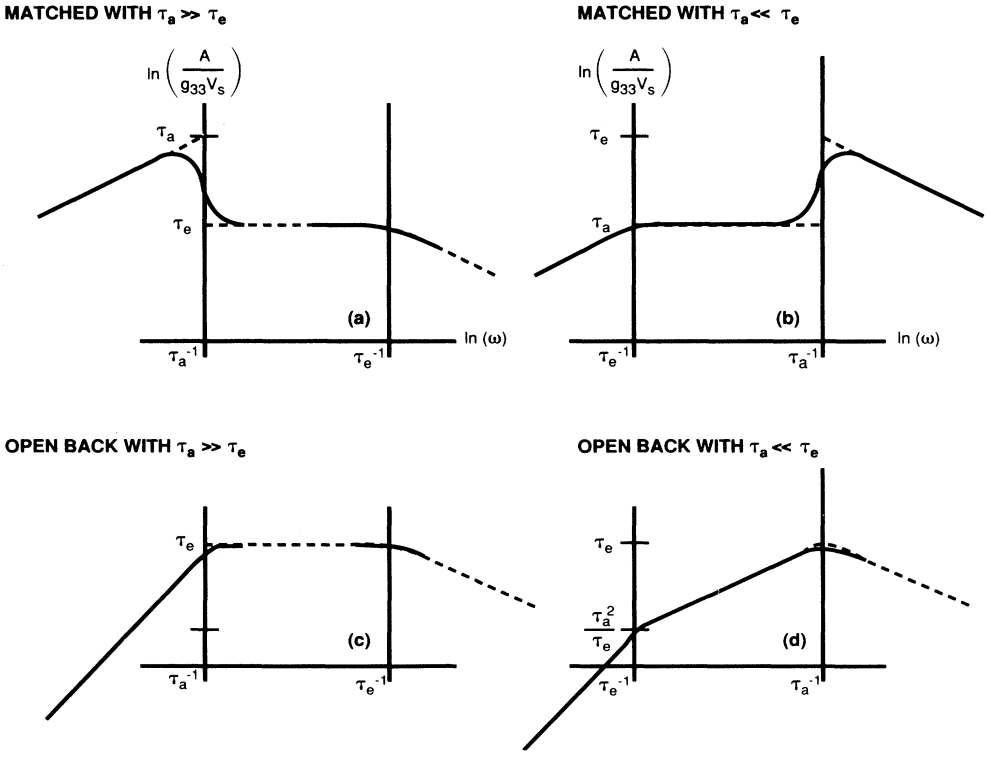

FIG. 5. Modified Bode plots for four possible transducer configurations, (a) and (b) are matched at both ends ($\Gamma_b = 0$), and (c) and (d) are open on the back ($\Gamma_b = -1$).

tion. Consequently, the high-frequency response will be the same for all transducers when $\omega \gg \tau_a^{-1}, \tau_e^{-1}$.

The slope of the high-frequency curves on the log-log plots of Fig. 5 is -1 which transforms to time integration. Similarly, the positive slopes seen on the low-frequency sides correspond to differentiation for a slope of $+1$ and double differentiation for a slope of $+2$. The open-backed configurations give the latter characteristics for $\omega \ll \tau_a^{-1}, \tau_e^{-1}$ which also represents a signal fall-off that is twice that of a matched transducer. In order to achieve a flat frequency response, one must be sure that the bandwidth of meaningful signals is within that region. The output will then be proportional to the signal itself, and the time domain output will trace the charge distribution.

The only open-backed arrangement with a flat signal response region in Fig. 5 is (c) where $\tau_a \gg \tau_e$. This is a transducer that is acoustically thicker than the arriving signal connected to a low impedance amplifier keeping τ_e very short. Outside the flat region, an output signal will be proportional to the integral, derivative, or second derivative of the arriving acoustic signal. If the frequency components containing charge distribution information overlaps a transition region, recovering the actual acoustic response may be difficult because of noise overwhelming the signal in the attenuated portion of the output spectrum.

3. *Multiple reflections*

A transducer with nonzero reflection coefficients at both interfaces has reflections originating from each boundary. This is the general case for any combination of materials with different acoustic impedances Z_a, such that

$$0 < |\Gamma_a, \Gamma_b| < 1 \tag{41}$$

whereby a fraction of the stress arriving at any time remains in the crystal and mixes with future signals. Lossless reflections would produce a signal at the fundamental resonant frequency of the crystal, resulting in a sharp frequency domain peak at $\omega = \tau_a^{-1}$. Finite reflection coefficients Γ_a and Γ_b broaden out the peak and mix incoming signals with only a fraction of previous signals.

Reflections from both surfaces can be treated by direct analogy to the previous two situations. The Fourier transform of the time domain, open circuit, voltage relation is multiplied by the transform of the *RC* detector circuit to give the total electrical response. The responses are summed over all time, weighted by the appropriate reflection coefficients, to produce the transducer response. Since only a portion of the arriving signal is seen across the transducer, the whole relation is multiplied by the transmission coefficient $1 + \Gamma_a$ at the front interface.

The resulting time domain expression for the open circuit voltage across the crystal is

$$V_i(t) = g_{33} v_s (1 + \Gamma_a) \int_0^{\tau_a} \sum_{n=0}^{\infty} (-\Gamma_a \Gamma_b)^n \{T(t + 2n\tau_a) + \Gamma_b T[t + (2n+1)\tau_a)]\}\, dt \tag{42}$$

and its associated Fourier transform

$$V_i(\omega) = \frac{g_{33} v_s (1 + \Gamma_a)}{j\omega} \left([T(\omega) + \Gamma_b T(\omega) e^{-j\omega\tau_a}] \sum_{n=0}^{\infty} (-\Gamma_a \Gamma_b)^n e^{-2nj\omega\tau_a} \right) \tag{43}$$

which can be simplified by solving the sum exactly to yield

$$\frac{V(\omega)}{T(\omega)} = \frac{g_{33} v_s (1 + \Gamma_a)}{j\omega} \left(\frac{1 + \Gamma_b e^{-j\omega\tau_a}}{1 + \Gamma_a \Gamma_b e^{-2j\omega\tau_a}} \right) \tag{44}$$

and has a pole when $\Gamma_a \Gamma_b = -1$. This would be the response of a perfectly mismatched transducer which is a resonator at the fundamental frequency $f_0 = \pi/\tau_a$. This could never occur in practice since it implies that the transducer is free-standing. In a more realistic matching situation, the transducer is loaded, at least on one side, making the relation stable and not resonant.

The amount of ringing depends on the size of both reflection coefficients as expected from (44). When the limiting cases of $\Gamma_a = 0$, and $\Gamma_b = 0$ or $\Gamma_b = -1$, there are no oscillations, and the results are the same as in Fig. 5. However, the loci of solutions for finite Γ_a and Γ_b are between the two extrema, with peaks near the resonant frequency and whose widths depend on the reflection coefficients.

The open-circuit frequency domain response is convolved with the detector response. The magnitude then gives the result

$$A(\omega) = \left| \frac{V_0(\omega)}{T_i(\omega)} \right| = \frac{g_{33} v_s \tau_e (1 + \Gamma_a)}{\sqrt{1 + (\omega\tau_e)^2}} \left| \frac{1 + \Gamma_b e^{-j\omega\tau_a}}{1 + \Gamma_a \Gamma_b e^{-2j\omega\tau_a}} \right| \tag{45}$$

for the generalized frequency domain impulse response of an acoustic transducer sandwiched between a delay line and an absorber at the back. The resonant configuration gives a large response to signal components near τ_a^{-1}, but attenuates lower-frequency components and superimposes a damped oscillation over the signal.

V. ACOUSTIC RESPONSE

Electrostatic force exerted on the material due to an applied field depends on the charge associated with that field, and the electrostriction coefficient γ, defined as[17,18]

$$\gamma = \epsilon (1 + c_a), \tag{46}$$

where c_a is a dimensionless material constant, defined by

$$c_a = \frac{\rho_{m0}}{\epsilon}\frac{\partial \epsilon}{\partial \rho_m} \tag{47}$$

with ρ_m representing the mass density. One can determine γ by measuring the electrostriction force with an applied field[17] and ϵ from the capacitance[19] to get a value for c_a. This number is typically much smaller than unity, making this a second-order correction.

The force per unit area on a thin sample with no embedded charge is found directly by

$$F_z = \gamma E_z^2 \tag{48}$$

for a uniform electric field E_z terminating on the sample boundary. Therefore, if $E_z(t)$ contains a dc and a time-varying component

$$E_z(t) = E_{\rm dc} + e_z(t) \tag{49}$$

then

$$E_z^2 = \tfrac{1}{2}E_{\rm dc}^2 + E_{\rm dc}e_z(t) + \tfrac{1}{2}e_z^2(t) \tag{50}$$

whereby the first term has no time dependence and shifts the equilibrium stress in the presence of localized charges. The perturbation field $e_z(t)$ generates a stress wave proportional to the electrostatic force exerted at the surface

$$f(t) = \gamma E_{\rm dc}e_z(t) + \tfrac{1}{2}\gamma e_z^2(t), \tag{51}$$

where $E_{\rm dc}$ is the surface field due to the applied dc voltage. The dc field term may be replaced by the surface charge

$$Q_s = \frac{\epsilon}{d}V_{\rm dc}, \tag{52}$$

where $V_{\rm dc}$ is the applied dc voltage used to calibrate the detection system.

A bulk sheet charge Q_s responds in the same way as one on the surface without the $e_z^2(t)$ self-field term. The stress density for an embedded sheet charge under excitation by a small field is found from (51) and (52),

$$T_q(t)_z = \frac{\gamma}{d}V_{\rm dc}e_z(t) + \frac{\gamma}{2}e_z^2(t), \tag{53}$$

for constant charge in the x-y plane. The calibration stress signal T_0 is the signal induced by a known applied voltage $V_{\rm dc}$,

$$T_0(t) = \frac{\gamma}{d^2}\left[(V_{\rm dc} + v_{\rm pulse})\, v_{\rm pulse}(t)\right], \tag{54}$$

allowing one to calibrate the detector to a known charge

$$Q_0 = \frac{\epsilon\,(V_{\rm dc} + v_{\rm pulse})\, v_{\rm pulse}(t)}{d^2} \tag{55}$$

being the surface charge due to capacitance and applied voltage. The resulting acoustic signal will be considered the calibration impulse response. The sign of the charge is also preserved since a negative charge launches an opposite directed stress wave from a positive charge that is distinguishable by the transducer.

If embedded space charge is distributed over an area within the bulk, the resulting pressure wave will be a time-varying signal across the sample. A one-dimensional charge distribution $\rho_q(z)_{x,y}$ will produce an acoustic stress perturbation in time and space $F_0(z,t)$ which launches an acoustic wave $T_i(z,t)$, as described in Sec. III,

$$F_0(z,t) = \frac{\gamma}{\epsilon}E_z(t)\rho_q(z)_{x,y}, \tag{56}$$

and propagates away at the velocity of sound to be received by the transducer. The constant term $\frac{\gamma}{\epsilon}$ is a material parameter that is nearly unity, and does not vary from one sample to the next. Once the stress produced from a known sheet charge layer is found, the detector can be calibrated to charge layers from different samples of the same material. A sample containing bulk space charge that is exposed to the impulsive perturbation field, produces a stress wave form that mimics the charge distribution. The distribution is then calibrated by the surface impulse response.

A. Surface sheet charge

The magnitude of the stress waves resulting from a sheet charge at the lower electrode interface is found by solving the wave equation with the boundary condition:

$$T_t + T_r = T_i, \tag{57}$$

where the subscripts t, r, and i indicate the transmitted, reflected, and incident stress waves. If the interface is abrupt, the transmitted stress will propagate, unperturbed, through the delay line.

The appropriate continuity condition is that the velocity $\dot{u}$ is constant across the boundary. This gives the result for a transmitted stress wave,[20]

$$T_t = T_i\frac{Z_{ad}}{Z_{ad} + Z_{as}} = T_i\frac{1+\Gamma}{2}, \tag{58}$$

where Z_a is the acoustic impedances in the sample s and delay line d. This states that the acoustic response of a sheet charge at the bottom surface has the same response of a sheet charge originating from within the bulk, allowing the calibration of an impulsive sheet charge within the sample to a surface sheet charge at the electrode. The acoustic mismatch between the sample under test and the acoustic delay line has no effect on the relative signal received. Consequently, as long as the impulse response is chosen with the same sample material, the electrical response of a single sheet charge can be used to deconvolve all subsequent charge distribution profiles.

The response to a sheet charge residing at the upper electrode will experience the same conditions for the magnitude of the generated signal. The portion of the initial stress which propagates in the direction of the sample, towards the detector, is the conjugate of that which propagates into the electrode. The upper electrode has an acoustic impedance Z_{au} so the transmitted signal from $z = d$ has

$$T_{td} = T_{id}\frac{Z_{as}}{Z_{au} + Z_{as}}(1+\Gamma). \tag{59}$$

Therefore, the second impulse due to the opposite electrode can be either enhanced or reduced by an impedance mismatch. If, however, the top electrode is matched with material having the same Z_a, then that second arrival impulse will be directly proportional to the charge, as is the impulse due to a charge on the lower electrode.

B. Bulk charge

The bulk charge is assumed to be a superposition of distributed sheet charges across the sample. Some digital signal processing is needed to recover the actual profile from the time domain signal if the transducer response is not flat with frequency. The surface sheet charge (per unit area) resulting from the perturbation electrical pulse across the insulator is the sum of the dc charge and the component due to the excitation:

$$Q_s = Q_{s0} + \frac{\epsilon}{d} E_z(t), \tag{60}$$

where Q_{s0} is the static surface charge and is either the result of internal charges or an externally applied voltage.

If the excitation field is small by comparison to the static internal field, then a buried charge, and its subsequent images on the outer surfaces, will generate signals proportional to their charges. This has been performed with an embedded electrode in a sample of PMMA with the results shown in Fig. 6. A thin aluminum sheet, 10 μm thick, was glued between two sheets of PMMA, one 6.4 mm and the other 2.9 mm thick. A 15-kV dc voltage was applied at the center electrode while the outer two surfaces were grounded. The resulting wave forms are shown. The time data show the result of the sample with applied voltage superimposed on the same sample with zero volts applied in order to visualize the actual response.

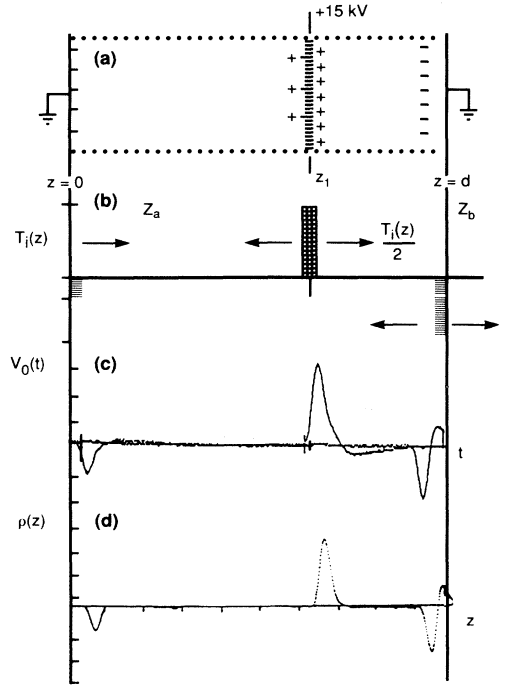

FIG. 6. Demonstration of the ESAW principle: (a) Q_{s1} is an imbedded sheet charge at $z = z_1$, with image charges Q_{s0} and Q_{sd} on the electrodes, (b) the resulting pressure wave signal after the excitation pulse, (c) an actual voltage detected by the transducer system, and (d) the resulting deconvolved charge profile.

In this example, the voltage was applied through a 100-MΩ resistor to the aluminum sheet. The capacitance had been approximated by assuming the electrode area is 7 cm^2 and the permittivity is $3.7\epsilon_0$, giving approximately 0.8 pf. This makes the RC time constant of the system very long with respect to the pulsewidth $\Delta t = 10^{-7}$ sec,

$$RC = 8 \times 10^{-5} \text{ sec} \gg 10^{-7} \text{ sec}. \tag{61}$$

The embedded positive charge Q_{s1} is located at z_1. Image charges Q_{s0} and Q_{sd} appear at the front and back electrodes under short circuit conditions as seen in (c) and (d) of Fig. 6. The stimulated pulses propagate out the insulator, through the electrodes, into the piezoelectric transducer, producing a voltage wave form $V_s(t)$. The signal is delayed by the lower electrode in order to separate the acoustic signal from electronic noise from the voltage pulse. This voltage wave form was amplified, detected, and recorded by the digitizing oscilloscope.

The first and second peaks of Fig. 6(c) are true indications of the characteristic charges, however, the signal due to the top electrode, $z = d$, is obscured by an immediate reflection at that surface. Consequently, to find the surface charge at both electrodes, two tests were performed, one with one side up, then another with that same side down. The two wave forms were compared to provide a measure of the actual charges at the surface on each side under short-circuit conditions and a redundant test for the bulk charge in between.

The area under the processed wave form [Fig. 6(d)] is proportional to the relative total charge in that portion of the bulk, whether it lies in a single sheet or is distributed. The total signal scales directly with pulse field as well as embedded charge, so it is proportional to the impulsive voltage and inversely proportional to the sample thickness.

The signal in Fig. 6 is the response of a 5.28-mm PMMA sample with 10-kV dc excitation. The filter cutoff frequency was selected at 10 MHz to eliminate most of the noise introduced by the system. The measured charges at each electrode, found by integrating under the peaks, were determined to be -8.0 and 24.2 nC/cm^2 at $z = 0$ and $z = z_0$, respectively. The actual charge density was found by assuming $\epsilon = 3.7\epsilon_0$, resulting in expected values of -7.65 and 24.4 nC/cm^2, both values are within 5%. The following section describes how a calibrated charge distribution is obtained by deconvolution with reference to a known sheet charge.

VI. EXPERIMENTAL CALIBRATION

The wave form resulting from a sheet charge layer was taken as the impulsive system response. The out-

put waveform of Fig. 7 is from a 0.528-cm-thick PMMA sample with a dc potential of 10 kV applied and no internal space charge. The top curve is the excitation input voltage pulse. The lower curve is the delayed output from the matched transducer made of lead zirconium titanate (PZT) sandwiched between a brass delay line and absorber. The initial pulse arrived at the transducer after 4.38 μsec and the second pulse arrives 1.94 μsec later. Thus, the velocity of sound in the sample is 2.72 mm/μsec, a value in agreement with the literature.

The first 1.5 μsec of this wave form was used as the impulse time function to deconvolve the whole wave form. The result is seen in Fig. 8 after averaging with a 10-MHz filter. The small amount of structure in the region between the two electrode peaks is due to the associated error. In this calibration example, the surface charge peaks were due to a 10-kV applied dc and $\frac{1}{2}V_p = 0.75$ kV from the pulse. Therefore, the applied E field, $E = 20.4$ kV/cm, producing a surface sheet charge density, $\sigma_s = 6.67$ nC/cm^2.

The known surface sheet charge calibrates the deconvolved charge distribution allowing one to plot the charge profile in real units of charge density, nC/cm^3. The fast Fourier transform routine used in this experiment returns a constant value of $\pi/2$ as the integral of the impulse signal deconvolved with itself. A charge distribution is proportional to the charge layer of thickness, $v_s\delta_d t$, where $\delta_d t$ is the digitizing interval, equal to 5 nsec for the recording scope used. The scaled output from the deconvolution is multiplied by the constant

$$\frac{2\sigma_s}{\pi v_s \delta_d t} \tag{62}$$

at every point in the output data string. This scale factor is determined for each sample and accounts for all the parameters for a particular sample, including the velocity of sound, thickness, and electrostriction coefficient.

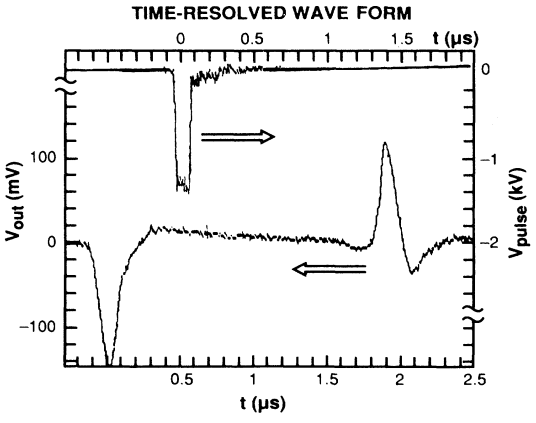

FIG. 7. Voltage pulse input V_{pulse} (top) and amplified transducer output, V_{out} (bottom); applied pulse precedes the acoustic response by the coupling delay of 4.38 μsec. The surface charges result from an applied dc voltage of 10 kV across a 5.28-mm PMMA slab with no internal charge distribution.

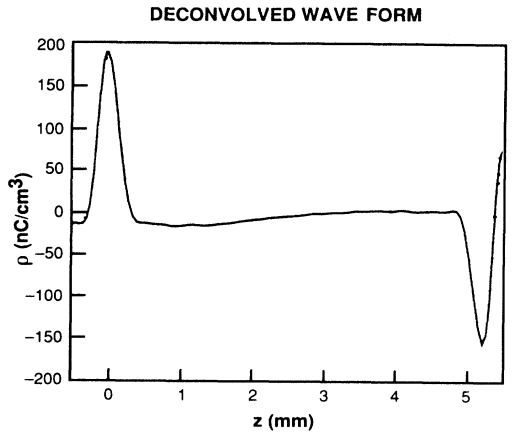

FIG. 8. Deconvolved and filtered wave form, scaled to the selected impulse response. Area under the peak, $Q_s = 6.67$ nC/cm^2.

Throughout this discussion, the linearity of the material has been assumed. Signals may not exceed the limits of linear stress-strain relations for the analysis to be valid. Starting with the yield stress for low density polyethylene as an example, we find that $T_{\text{yield}} = 700$ N/cm^2.[14] This may be compared to the stress induced by electrostatic forces. Consider a dc field much larger than any which will be performed in this study, 100 kV/mm:

$$T_i = \frac{\gamma}{d^2}V_{\text{dc}}^2 = 0.02 \text{ N/cm}^2 \tag{63}$$

assuming $\gamma = \epsilon = 2.3\epsilon_0$, which is approximately 5 orders of magnitude lower than the yield stress, justifying the assumption of acoustic linearity.

A sheet charge results in a signal that is 120 nsec wide, corresponding to 324 μm in the sample. One can say that the resolution is good to approximately half the full width at half maximum, giving a real spatial resolution in PMMA of 162 μm. The sensitivity is found from the signal-to-noise ratio of the output signal. As seen in Fig. 8, the central region zero charge is limited to within approximately 8 nC/cm^3. The resulting figure of merit for the detection system is the product of these two values, giving a sensitivity-resolution value of 130 pC/cm^2. This value represents the smallest detectable sheet charge using this system.

VII. CONCLUSIONS

The ESAW method for measuring one-dimensional space charge distributions has been shown to work in millimeter-thick organic dielectrics. One advantage of this method over other pressure wave propagation techniques is the voltage gain facilitated by the transducer. In a system where the acoustic wave is propagated through the sample, as with the laser-induced pressure pulse,[7] for example, the simple displacement current is detected externally. With the ESAW method, the acoustic signal

produces a voltage that is amplified by the factor g_{33} as it propagates through the piezoelectric medium.[15] The gain is usually much larger than the coupling loss between the boundaries, making the ESAW method a potentially superior space-charge profiling system.

The resolution is limited, in principle, by the ability to make a detector system that is sufficiently broad-banded. Within the bandwidth, the smallest detectable signal is limited by noises in the detection system. The strength of an originating signal is proportional to the charge density times the spatial resolution. We may use a figure of merit, equal to this product, as a means for comparison. For the present system, the figure of merit is 130 pC/cm^2, which is lower than for any other acoustic technique.[11]

One may extrapolate the possibility of scaling down the system to profile micrometer-thick films. The limiting factors are the velocity of sound in the material with respect to the speed of the perturbation and the detection equipment, as well as the maximum field that may be applied without causing dielectric breakdown.

The velocity of sound in most inorganic materials is higher than in organic insulators by approximately a factor of 2–3, further reducing the resolution capability. On the other hand, interfaces may be grown *in situ* with the film, making planar contacts for an ESAW experiment. A flat acoustic frequency response is the most ideal receiver, and may be achieved by having the electrical and acoustic time constants of the detector separated by several orders of magnitude around the inverse frequency range of interest. This would be most easily achieved by using a piezoelectric substrate that is much thicker than the film, loaded into a low-impedance amplifier, being sure that the electrical time constant is much shorter than the minimum desired resolution width divided by the velocity of sound in the material.

A second way to accomplish the needed broadband detector would be to deposit a piezoelectric film that is much thinner than the film of interest. This would be experimentally more difficult since a conducting interlevel layer must be deposited and a thick matching layer should be deposited on top of that. Otherwise, the detector will operate in a differential mode, requiring more careful signal processing to obtain the charge distribution profile.

In conclusion, one can design an ESAW system using any piezoelectric material as long as the dimensions and interfaces are controlled. This technique could be useful for characterizing materials that exhibit space-charge accumulation. It may be used in conjunction with space-charge-limited current or time-of-flight experiments to gain a further understanding of the electron dynamics in semi-insulating materials.

ACKNOWLEDGMENTS

I wish to gratefully acknowledge the assistance of Professor Stephen D. Senturia, Chatan M. Cooke at the MIT High Voltage Research Laboratory, and James R. Melcher.

[1] M.A. Lampert and P. Mark, *Current Injection in Solids* (Academic, New York, 1970).
[2] J. Sworakowski and S. Nespurek, IEEE Trans. Electric. Insul. **24**, 223 (1989).
[3] V. Adamec and J.H. Calderwood, IEEE Trans. Electric. Insul. **21**, 389 (1986).
[4] M. Ieda, IEEE Trans. Electric. Insul. **19**, 162 (1984).
[5] D. Adler, in *Physical Properties of Amorphous Materials*, edited by D. Adler, B.B. Schwartz, and M.C. Steele, (Plenum, New York, 1985).
[6] T.J. Lewis, IEEE Trans. Electric. Insul. **21**, 289 (1986).
[7] J. Lewiner, IEEE Trans. Electric. Insul. **21**, 351 (1986).
[8] C.M. Cooke, K.A. Wright, N. Takasu, J.B. Bernstein, and E. Gollin (unpublished).
[9] J.B. Bernstein and C.M. Cooke, IEEE Trans. Electric. Insul. (to be published).
[10] J.B. Bernstein and C.M. Cooke, IEEE Trans. Electric. Insul. (to be published).
[11] J.B. Bernstein, Ph.D. thesis, Massachusetts Institute of Technology, 1990.
[12] T. Takada, T. Maeno, and H. Kushibe (unpublished).
[13] T. Maeno, T. Futami, H. Kushibe, T. Takada, and C.M. Cooke, IEEE Trans. Electric. Insul. **23**, 433 (1989).
[14] *Handbook of Chemistry and Physics*, 58th ed., edited by R. C. Weast (CRC, Orlando, FL, 1977).
[15] G.S Kino, *Acoustic Waves: Devices, Imaging, and Analog Signal Processing* (Prentice Hall, Englewood Cliffs, N.J., 1987).
[16] H.A. Haus and J.R. Melcher, *Electromagnetic Fields and Energy* (Prentice Hall, Englewood Cliffs, N.J., 1989).
[17] K. Nakamura and Y. Wada, J. Poly. Sci. **9**, 161 (1971).
[18] M. Oshiki and E. Fukada, J. Mat. Sci. **10**, 1 (1975).
[19] J.R. Melcher, *Continuum Electromechanics* (MIT Press, Cambridge, MA, 1981).
[20] H.J. Pain, *The Physics of Vibrations and Waves*, 3rd ed. (Wiley, London, 1983).